

H II REGIONS IN SPIRAL GALAXIES:
SIZE DISTRIBUTION, LUMINOSITY FUNCTION, AND NEW ISOCHRONE DIAGNOSTICS OF
DENSITY WAVE KINEMATICS

M. S. OEH

Lowell Observatory, 1400 W. Mars Hill Rd., Flagstaff, AZ 86001

JEFFREY S. PARKER^{1,2}

Whitman College, Walla Walla, WA 99362

VALERIE J. MIKLES^{1,3}

Johns Hopkins University, Dept. of Physics and Astronomy, Baltimore, MD 21218

AND

XIAOLEI ZHANG

Naval Research Lab, Remote Sensing Division, 4555 Overlook Ave., SW, Washington, DC 20375

Accepted to the ASTRONOMICAL JOURNAL 16 June 2003

ABSTRACT

We investigate the relationship of the H II region luminosity function (H II LF) to the H II region size distribution and density wave triggering in grand-design spiral galaxies. We suggest that the differential nebular size distribution is described by a power law of slope ~ -4 , with flattening at radii below ~ 130 pc. This contrasts with the conventional exponential description, but it is physically and quantitatively consistent with the typical observed value of -2 for the H II LF slope.

We have developed an interactive code that computes spatial isochrones for the evolving loci of spiral density waves in disk galaxies. This allows comparison of the nebular spatial distribution with the spatial isochrones for simple rotation curve parameters. Our comparisons for four grand-design galaxies suggest that the corotation radius r_{co} coincides with the outer ends of the star-forming arms. This value for r_{co} yields the best spatial correspondence between the H II regions and the isochrones, and also appears to yield a coincidence between the Inner Lindblad Resonance with the radial onset of star formation in the arms. Thus, *we suggest that isochrones offer a new, simple, and effective technique for determining r_{co} , and thus the spiral pattern speed.* However, application of the isochrones also demonstrates that evolution of the nebular population is difficult to spatially isolate in these galaxies.

Subject headings: H II regions — galaxies: fundamental parameters — galaxies: kinematics and dynamics — galaxies: spiral — ISM: kinematics and dynamics

1. INTRODUCTION

The H II region luminosity function (H II LF) is an important diagnostic of star formation properties in galaxies. It is a fairly straightforward parameter to determine for nearby galaxies (e.g., Kennicutt, Edgar, & Hodge 1989; Banfi et al. 1993; Rozas, Beckman, & Knapen 1996a; Thilker et al. 2002), and is usually presented in the differential form as a power law:

$$N(L) dL = A L^{-a} dL , \quad (1)$$

where $N(L) dL$ is the number of nebulae with H α luminosities in the range L to $L + dL$. Occasionally, the cumulative H II LF is given, but we note that the differential form is a more powerful diagnostic of the underlying properties (Cioffi & Shull 1991).

In an earlier paper (Oey & Clarke 1998, hereafter Paper I), we modeled the behavior of the H II LF, and identified ways in which it can be used to examine the current properties of massive star formation and recent ($\lesssim 10$ Myr) star formation history. We assumed a power-law distribu-

tion in N_* , the number of ionizing stars per object:

$$N(N_*) dN_* = B N_*^{-\beta} dN_* . \quad (2)$$

We then performed Monte Carlo simulations, in which we draw N_* from this distribution, and also draw the individual stellar masses from a Salpeter (1955) initial mass function (IMF). These models showed that reported variations of the measured slope a (equation 1) in different environments *do not require varying β* , the slope of the N_* distribution (equation 2), but rather, can be explained by variations in the star formation history and the upper cutoff in the N_* distribution. An important feature is that stochastic effects for objects with small N_* cause a flattening in the H II LF below a certain luminosity L_{sat} . Sparse clusters subject to this effect are termed “unsaturated” with respect to the IMF, and clusters with higher N_* we call “saturated”. We identified L_{sat} with the H α luminosity associated with the most massive star in the IMF, although we refer readers to Paper I for a complete discussion.

A basic test on the nature of the H II LF is its relation to the size distribution of the H II regions. Although the

¹Participant in the 1999 STScI Summer Student Program.

²Present address: University of Colorado, Dept. of Aerospace, Engineering Sciences, Boulder, CO 80309

³Present address: University of Florida, Dept. of Astronomy, P.O. Box 112055, Gainesville, FL 32611

H II LF has empirically been described by a power law, the corresponding size distribution has been described by an exponential law (van den Bergh 1981; Hodge 1983, 1987). As discussed above, Paper I found that the slope breaks and other features in the H II LF are nevertheless best explained by a simple power law in N_* (equation 2 of Paper I). Therefore we should naively expect the size distribution to also follow a power-law distribution. In §2 below, we examine whether observations of the H II region size distribution are consistent with a simple power-law relationship.

Another test on the nature of the H II LF addresses its evolutionary properties. The models constructed in Paper I included the evolution of the H II LF resulting from a single burst creation scenario. In Figure 1, we show representative zero-age and 7 Myr models (Figures 2a and c of Paper I). The zero-age model shows the flattening below L_{sat} . As time goes by, the entire H II LF shifts to lower L . However, when considering a fixed range of L , this can result in an apparent elimination of the slope break in strongly evolved populations, due to the differential fading effect. If this model turns out to be correct, it would then be possible to distinguish, for example, between an older nebular population where high-luminosity objects were created in a single burst, and continuous creation of low-luminosity H II regions.

Paper I applied these results to observations of arm and interarm regions of grand design spiral galaxies, suggesting that arm populations represent the current burst of star formation, while interarm objects represent an aged population remaining in the wake of the spiral density waves. Observations in the literature sometimes suggest that interarm populations show a slightly steeper H II LF than the arm populations (e.g., Kennicutt et al. 1989; Rand 1992). This phenomenon can be explained by the two-slope structure in the zero-age models, which will cause a slope measurement to be flatter when fitted over L below L_{sat} (see Figure 1). In contrast, the evolved populations show the intrinsic slope of the high- L regime. Figure 5 of Paper I shows that this interpretation of evolution between the arm and interarm H II regions is consistent, in all cases, with available observations of six grand design spiral galaxies.

Observations of the H II LF in the literature to date have been subjectively and coarsely binned into the arm and interarm categories. A more powerful test of this evolutionary scenario would be to rebin the H II regions more quantitatively into regions corresponding to fixed age ranges behind the leading edge of the spiral arms, as inferred from the spiral arm pattern speeds. We might then be able to examine the competing contributions in interarm regions, of aging nebular populations versus bona fide interarm star formation. These are our motivations for carrying out the studies described in §3. As an important by-product of this study, we developed a technique that compares nebular positions with spatial isochrones for the spiral density waves. This offers a new method for locating the corotation resonances in spiral galaxies, and is described in §4.

2. THE FORM OF THE H II REGION SIZE DISTRIBUTION

As mentioned in the Introduction, the conventional parameterization of the H II region size distribution as an exponential (e.g., van den Bergh 1981; Hodge 1983, 1987)

is intuitively at odds with the power-law form of the H II LF. Since the H II LF's behavior appears to be fairly well-understood (e.g., Paper I), it is important to reexamine the size distribution within the same framework, since they are physically related. In particular, we might also expect the size distribution to follow a power law of the form,

$$N_r(R) dR \propto R^{-b} dR , \quad (3)$$

where R is the nebular radius. This has indeed been suggested for some galaxies (e.g., Pleuss, Heller, & Fricke 2000).

Since the nebular H α luminosity L is integrated from the nebular volume emission, we should expect $L \propto R^3$ and $\frac{dL}{dR} \propto R^2$. Therefore, the differential size distribution should be:

$$N_r(R) dR = N(L) \frac{dL}{dR} dR \propto R^{2-3a} dR . \quad (4)$$

Hence we find that the slopes a and b of the H II LF and size distribution, respectively, are related as $b = 2 - 3a$. For the usual value $a = 2$ found for the high-luminosity, “saturated” H II regions, we therefore predict a corresponding size distribution having $b = 4$.

As mentioned earlier, a turnover in the H II LF caused by stochastic effects for “unsaturated” objects occurs at a luminosity L_{sat} . Since L_{sat} is associated with the most massive stars in the IMF, their Strömgren radius R_{sat} should be a corresponding inflection point in the size distribution. This flattening at small R can mimic an exponential distribution. For the most massive stars, stellar atmosphere models suggest $\log L_{\text{sat}}/\text{erg s}^{-1} \sim 38.0$ to 38.5 (Schaerer & de Koter 1997; Vacca, Garmany, & Shull 1996; Panagia 1973), implying $R_{\text{sat}} \sim 130$ pc for a density of 1 cm^{-3} . This estimate for R_{sat} should be taken as an upper limit, since the density is likely to be higher in the actual, central star forming area.

We can now compare observations of the H II region size distribution to our predictions for slope $b = 4$, with a flattening in R below $\log R_{\text{sat}}/\text{pc} \sim 2.1$. We refitted the nebular diameter distributions with power laws for a number of galaxies in the literature. Since size determinations can be sensitive to different methods, and thus to ensure relatively consistent comparisons, we used data from only two groups of investigators: the IAC–Hertfordshire collaboration (Knapen et al. 1993; Rozas et al. 1996b; Knapen 1998), and Youngblood & Hunter (1999). Hodge's group (e.g., Hodge et al. 1994); Miller & Hodge 1994; Hodge et al. 1999) and Petit's group (e.g., Petit 1993, 1996, 1998) have contributed many studies of H II region size distributions; however, their target galaxies generally do not offer enough objects to adequately sample the nebular size distribution at $\log D/\text{pc} > 2.4$, where D is the nebular diameter. Likewise, we include only the three galaxies from the Youngblood & Hunter (1999) sample that provide adequate sampling in this regime.

Figure 2 shows the size distributions for the nine galaxies listed in Table 1. We fitted power law slopes for $\log N(D)/\text{pc} \geq 2.3$, with the bins weighted by \sqrt{N} . The IAC–Hertfordshire galaxies are grand design spirals and the Youngblood & Hunter galaxies are Magellanic irregulars. Both these sets of galaxies have H II LFs extending to

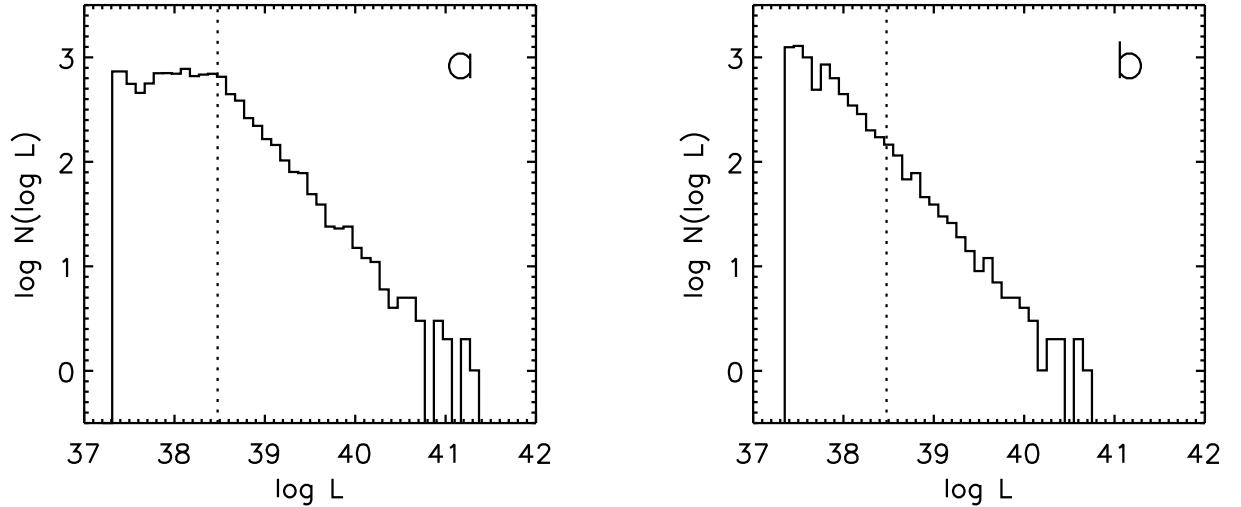


FIG. 1.— Model H II LFs: (a) zero-age; and (b) evolved single-burst, from Oey & Clarke (1998; Figures 2a and c). The dotted line marks L_{sat} .

high luminosities, consistent with no upper cutoff in luminosity. Our fits to the size distributions therefore should not be influenced by possible truncation at the upper end of the H II LF. It appears that the H II region diameter distributions shown in Figure 2 are consistent with power laws in the given regime. Objects with smaller diameters show a flattening in the size distribution, qualitatively consistent with the flattening in the H II LF for statistically unsaturated objects.

The small dynamic range and small number statistics cause some ambiguity and large uncertainties in the fitted slope $-b$, as shown in Figure 2. We also caution that we cannot rule out the existence of systematic effects. Nevertheless, the average slope, weighted inversely by the uncertainties, is $\langle b \rangle = 4.12$ with a standard deviation of 0.90. This preliminary result agrees with the value predicted above of $b = 4$. Figure 2 also shows that the turnover in the diameter distribution is also consistent with the predicted value of $\log D/\text{pc} \sim 2.4$. *We therefore suggest that the H II region size distribution is intrinsically described by a power-law function* in the regime beyond the turnover, consistent with its physical relation to the H II LF. While consistent functional forms are expected for the size distribution and H II LF, further confirmation of the empirical power law for the former is desireable, with attention to systematic uncertainties in size determinations.

3. TESTING FOR AN EVOLVING H II LF

Based on Paper I, we approximate that the H II regions found along the leading edge of spiral arms represent the youngest, zero-age population of objects. H II regions behind the leading edge therefore represent a somewhat older population remaining in the wake of the spiral density wave. If the galactic rotation curve and spiral arm pattern speed are known, it is in principle possible to estimate the ages of objects based on their location with respect to the

leading edges of the spiral arms. This would also assume that the velocities of the H II regions do not deviate significantly from the galactic rotation curve during the passage of the density wave.

We have developed a code that computes spatial isochrones from the rotation curve, given the current locus of the spiral arms. We defer discussion of the code and spiral arm kinematics until §4 below, and here use the spatial isochrones to search for evolutionary features as predicted in Paper I. We examined four of the grand design spiral galaxies studied in Paper I, while the two remaining galaxies included in that paper, NGC 3631 and NGC 6814, did not have a simple two-arm structure suitable for this analysis. Figure 7 below shows H α images of the galaxies: M51 (Rand 1992), M100 (Knapen et al. 1993), NGC 157, and NGC 6951 (Rozas et al. 1996). Five sets of spatial isochrones are calculated for each of the two dominant arms in these galaxies, calculated at intervals of 12 Myr. The color scheme for times $-12, 0, 12, 24$, and 36 Myr are: red, green, yellow, yellow, red for one arm; and blue, yellow, green, green, blue for the other. The zero-age isochrones correspond to an actual spatial fit to the arm positions. The adopted corotation radius is shown with the black dashed line, and the inner and outer Lindblad resonances are shown in the solid and dotted black lines, respectively, assuming $m = 2$ spiral arms for these galaxies.

Unfortunately, it appears that the isochrone spatial separation that is sensitive to the nebular evolutionary timescale is of order the spatial scatter of the objects along the spiral density wave. Figures 7a – c show that the best-defined arms are enclosed within the -12 to $+12$ Myr isochrones, but show a spatial scatter that precludes further distinction. NGC 6951 is an exception (Figure 7d), showing larger separation between the isochrones that also corresponds to the nebular spatial distribution.

TABLE 1
REFERENCES FOR GALAXY DIAMETER DISTRIBUTIONS

Galaxy	Type ^a	Reference
M100	Sc(s)I	Knapen (1998)
NGC 157	Sc(s)I-II	Rozas et al. (1996b)
NGC 1156	SmIV	Youngblood & Hunter (1999)
NGC 2366	SBmIV-V	Youngblood & Hunter (1999)
NGC 3631	Sbc(s)II	Rozas et al. (1996b)
NGC 4214	SBmIII	Youngblood & Hunter (1999)
NGC 6814	Sbc(rs)I-II	Knapen et al. (1993)
NGC 6764	SBbc(s) ^b	Rozas et al. (1996b)
NGC 6951	Sb/SBb(rs)I.3	Rozas et al. (1996b)

^aFrom Sandage & Tamann 1987.

^bType as listed by Rozas et al. (1996b).

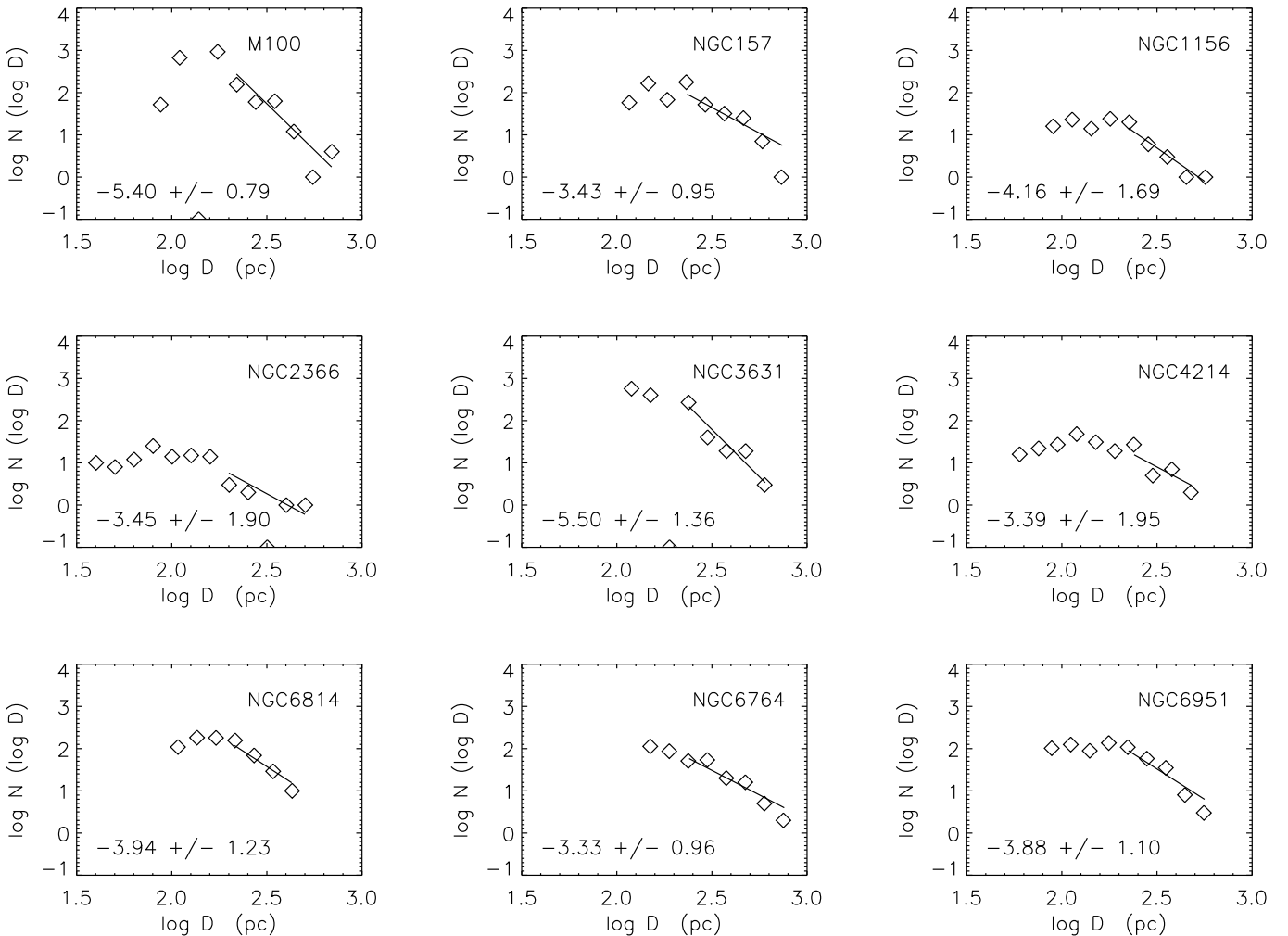


FIG. 2.— Differential H II region diameter distributions for galaxies in Table 1, fitted with power laws for $\log D/\text{pc} \geq 2.3$. The fitted values of $-b$ and standard deviation are shown [note that the fitted slope for $\log N(\log D)$ vs. $\log D$ is $1 - b$]. Empty bins are shown as $\log N(\log D) = -1$.

Figures 3 – 6 show the H II LF for sub-groups of H II regions binned within isochrones for -12 to $+12$ Myr (panels *a*); 0 to 24 Myr (panels *b*), and 12 to 36 Myr (panels *c*). As discussed above from Paper I, the H II LF naturally shows a break in slope below the high-luminosity power-law tail, that is caused primarily by the transition to unsaturated stellar clusters dominated by small-number statistics. For older nebular populations, this slope transition at L_{sat} is expected to shift toward lower luminosities, while the high-luminosity power-law slope remains the same (Figure 1 above; Paper I). The vertical dotted line in these figures shows the luminosity bin where we estimate L_{sat} to occur for the youngest binning; this value is plotted for reference, and remains constant between the three H II LF subsets for each galaxy.

It is apparent in Figures 3 – 6 that the location of L_{sat} is essentially indistinguishable between the three subsets. The transition point generally appears to be more ambiguous in the oldest binnings (panels *c*) as compared to the youngest (panels *a*), but more galaxies must be examined to determine whether that pattern is real. If so, then it would be consistent with a greater contribution from evolved populations (Paper I). The ambiguities again reflect our discussion above, that the isochrones for these galaxies are insensitive to aging effects, since the spatial scatter is of order the separation for isochrones over the nebular evolution time scale.

A number of other factors probably also contribute to the insensitivity of the isochrones to aging effects. First, the models in Paper I (e.g., Figure 1 above) assumed the instantaneous creation of all objects in the H II LF, whereas triggering by the spiral density wave most likely has a finite timescale. Since most H II regions recombine on timescales of $\lesssim 10$ Myr, we would not expect any significant population to be visible at 24 Myr. For the most part, this is consistent with the fairly negligible $\text{H}\alpha$ emission at the 24 Myr isochrone for most of the arms in M51, M100, and NGC 157. NGC 6951 shows spatially more extensive star formation, with H II regions also seen along the 24 Myr isochrone; this therefore implies an extended timescale for star formation at any given location. An extended star-formation timescale is also equivalent to a spatial scatter for objects of any given age, as mentioned above. For the H II LFs, this will blur the distinction between the youngest subset and next-to-youngest. It may also be that the luminosity fading of the H II regions is even faster than our extreme model in Paper I (see Paper I, Figure 2*f*). Another factor that affects the quantitative comparison to the H II LF evolution is the uncertainty in identifying and fitting the locus of the zero-age density wave. Finally, our simple analytic description for the rotation curve and pattern speed are idealized forms that do not describe the details of the gas kinematics (see §4 below), which also affect the location of the spatial isochrones.

Thus, our test of the evolutionary features in the H II LF for these galaxies is inconclusive, though an upper limit on the evolutionary effects is indicated. For most of the galaxies, the spatial isochrones do not offer the necessary separation to isolate populations of H II regions triggered in the arm density waves.

4. LOCATING COROTATION WITH SPATIAL ISOCHRONES

We now describe our analysis of spatial isochrones, which offer some interesting insights on spiral arm kinematics.

While measurements of rotation curves are fairly straightforward, historically it has been much more difficult to estimate the spiral density wave pattern speed, or equivalently, to determine the location of the corotation radius. Several methods for determining the corotation radius or pattern speed have been proposed in the past. The earliest proposal was based on Lin’s (1970) conjecture that organized, two-armed spiral patterns exist only within the corotation circle, and that arms become more fragmented outside. Shu, Stachnik, & Yost (1971) were among the first to apply this conjecture to physical galaxies, placing the corotation where the distribution of H II regions is seen to end. Tremaine & Weinberg (1984) developed an approach for pattern speed determination based on measurement of surface brightness and velocity distributions of luminosity density tracers, assuming continuity in the tracer. Canzian’s (1993) method for determining corotation relies on the qualitative difference in the residual velocity field inside versus outside of corotation. Elmegreen, Elmegreen, & Seiden (1989) identified resonances through breaks in spiral arms, and Cepa & Beckman (1990) utilized the radial star formation efficiency. Elmegreen, Wilcots & Pisano (1998) determined corotation from the transition of the inward to outward streaming gas velocity. Finally, Clemens & Alexander (2001) used high-resolution spectroscopic data to find signatures of the pre- and post-shock gas across the spiral arms; this information determines the shock velocity, and hence, the pattern speed. In what follows, we explore a new approach that uses the nebular spatial distribution to constrain the corotation radius.

For a galaxy with a flat rotation curve, the corotation radius r_{co} is related to the angular pattern speed Ω_p as,

$$\Omega_p = \frac{v_{\text{circ}}}{r_{\text{co}}} \quad , \quad (5)$$

where v_{circ} is the circular velocity. Assuming that star formation is triggered by spiral density waves, the locus of the youngest H II regions essentially indicates the location of the density wave. As the nebulae age, their positions will be determined by both the spiral arm pattern speed and the galaxy’s rotation curve. It is therefore possible to determine spatial isochrones for a given galaxy, that represent the positions of objects that all formed simultaneously within a density wave.

Our code computes spatial isochrones, given an initial locus for the spiral arm pattern. The H II region positions are deprojected and converted to polar coordinates, and we fit the spiral pattern at the arm’s leading edge, using a polynomial function. We then compute spatial isochrones from the locus of the spiral arm pattern, rotation curve, and putative corotation radius. We assume a flat rotation curve, except for the innermost regions $r < r_{\text{circ}}$, where we assume $v \propto r$ (Table 2).

Our code includes a widget to easily adjust the assumed corotation radius. Varying r_{co} by hand, we found a value of r_{co} that determines a set of isochrones having a noticeable correspondence to the spatial configuration of the H II regions. These values of r_{co} turn out to correspond to the

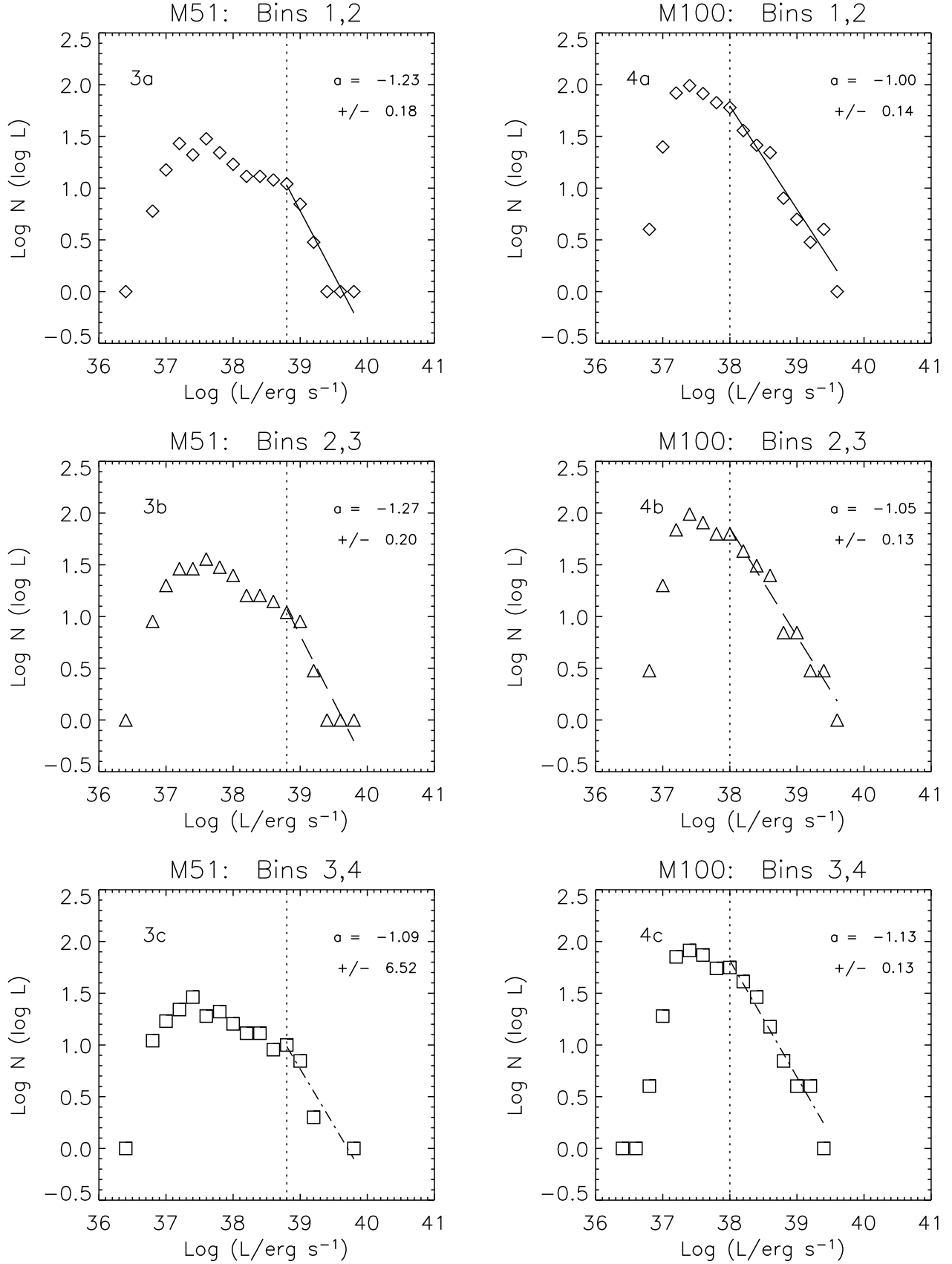
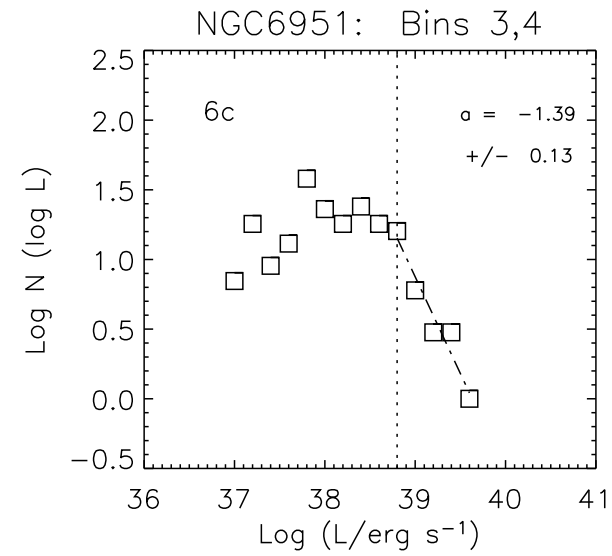
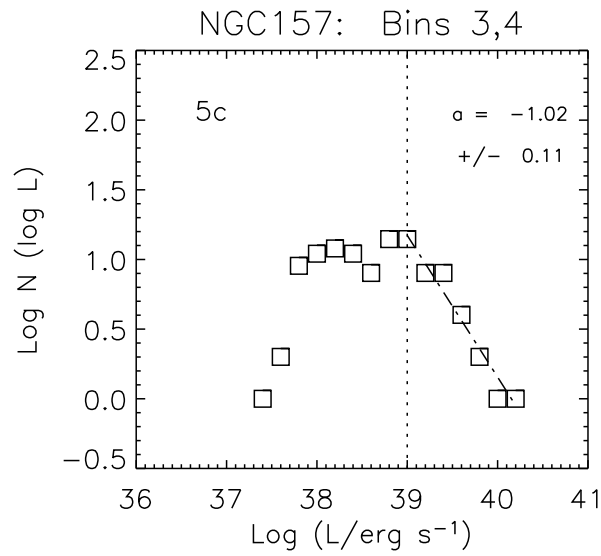
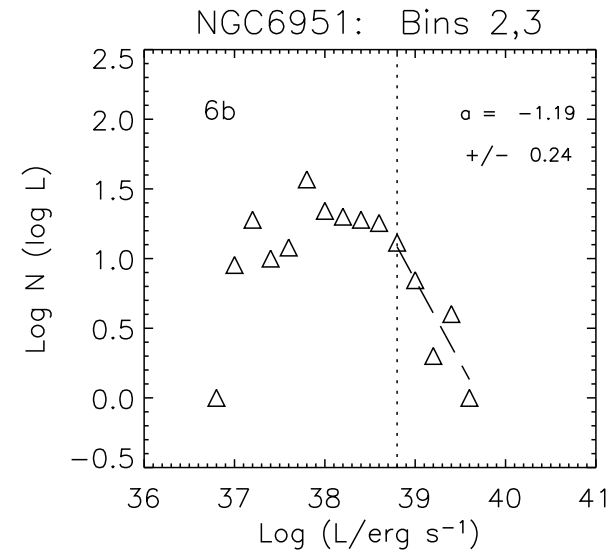
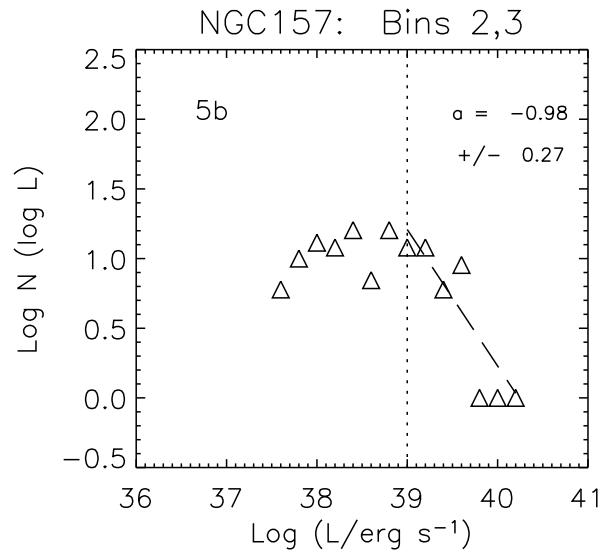
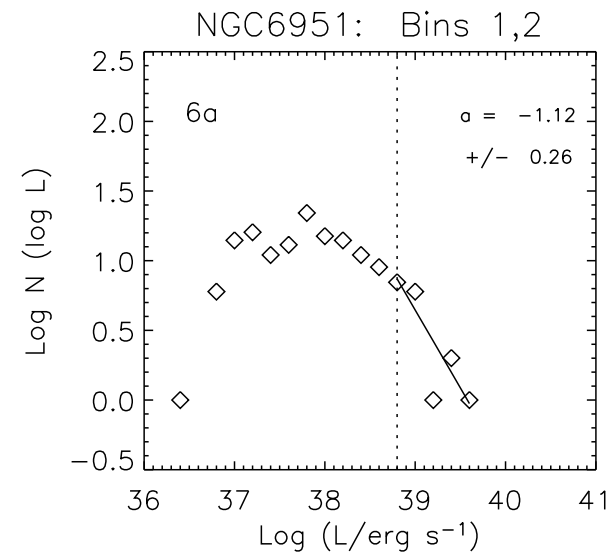
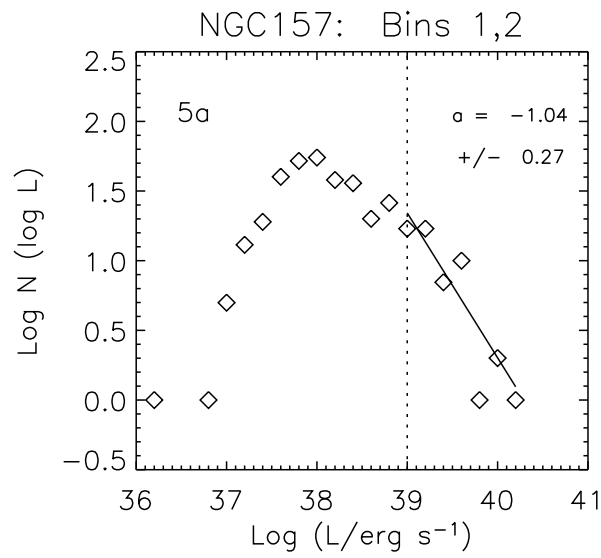


FIG. 3.— 6. — HII LFs for objects binned between isochrones for M51, M100, NGC 157, and NGC 6951. Panels *a*, *b* and *c* respectively show Bins 1 – 2 (–12 to +12 Myr), Bins 2 – 3 (0 – 24 Myr), and Bins 3 – 4 (12 – 36 Myr).



ends of the spiral arms in the star-forming disk. As we discussed above, other investigators (e.g., Shu et al. 1971; Rohlfs 1977; Kenney et al. 1992; Zhang, Wright, Alexander 1993) have identified r_{co} with the ends of the spiral arms in the past. For three of our four galaxies, Figure 7 shows that these values of r_{co} also yield inner Lindblad resonances (ILRs) that coincide well with the radial onset of significant star formation in the arms. Figure 7b also suggests a correspondence between the outer Lindblad resonance (OLR) and the edge of the star-forming disk in M100.

For all four galaxies, the regions near the ILRs display the characteristic “twin-peaks” morphology (Kenney et al. 1992) or “twin-peaks-plus-inner-bar” (Zhang et al. 1993), together with an annular zone between the twin peaks and the inner bar/nucleus that is swept clear of star formation. This combination of central morphologies is common among mid- to early-type galaxies, and is related to the orbital behavior of gas near the double inner Lindblad resonances that are present in these galaxies with high central potential wells (Zhang et al. 1993, and references therein), namely, the inner-inner-Lindblad resonance (IILR) and the outer-inner-Lindblad resonance (OILR). This morphology allows the effective central channeling of gas and fueling of nuclear activity. Note that our simplified assumed rotation curves yield only one ILR which presumably is located between the IILR and OILR of the actual rotation curves.

For M51 and M100, Figure 7 shows that setting r_{co} to the tips of the spiral arms causes the isochrones to bunch or converge, but not cross over, at azimuthal locations near large clumps of nebulae. These clumps are not confined within the isochrones, and extend to radii substantially beyond them; however, their azimuthal coincidence with the isochrone convergences strongly suggests that these loci are associated with dynamical triggering of the star formation. These patterns are most likely related to non-circular motions and asymmetry in the mass distributions. Indeed, both M51 (see García-Burillo et al. 1993) and M100 (García-Burillo et al. 1998) show evidence of an inner tri-axial mass distribution. It is also apparent in Figure 7 that the spatial isochrones only cover a fraction of the active star-forming regions in the disks, which again must be caused by non-circular kinematics. However, our experimentation with rotation curve parameters showed that to first order, our simple assumptions for the rotation curve (flat, with a linear inner portion) worked best in matching the H α morphology of the arms.

A counterexample is shown in Figure 8 for M51. One previous estimate for r_{co} in this galaxy is 9.6 kpc (Elmegreen et al. 1992). It is apparent that the isochrones do not correspond to the H II region positions as cleanly as in Figure 7a. The arms show a smooth, continuous morphology in the region around the suggested r_{co} , whereas the predicted isochrones change character and diverge.

Table 2 shows our assumed rotation curve parameters and our estimates for the r_{co} , ILR, and OLR. We now compare our results for r_{co} with those in the literature, in particular, estimates derived from kinematic models. There are no modeled estimates of r_{co} for NGC 6951.

4.0.1. M51

Our analysis suggests that the corotation radius is twice as large as most previous determinations for M51. Both morphological estimates (e.g., Vogel et al. 1993; Elmegreen et al. 1992; Knapen et al. 1992) and kinematic model estimates (García-Burillo et al. 1993b) found r_{co} of 126'' – 161'', in contrast to our estimate of 301''. We note that M51 is one of the few examples where the arm definition is narrow enough that the R -band and H α or CO observations can clearly distinguish the stellar arms from the new star-formation (Rand & Kulkarni 1993; García-Burillo et al. 1993a). At corotation, the youngest regions should switch from the inside edge of the arm to the outside; yet the data shown by Rand & Kulkarni (1990) and García-Burillo (et al. 1993a) show no evidence for this transition at the smaller r_{co} suggested in the past.

4.0.2. M100

For M100, our corotation radius is larger than previous estimates, but by a smaller margin. Estimates by García-Burillo et al. (1998) and Canzian & Allen (1997), based on kinematic modeling, and also Elmegreen et al. (1992) all agree fairly well with the range of 82'' – 114'' estimated for r_{co} by Sempere et al. (1995). Our estimate of $r_{\text{co}} \sim 154''$ is larger, but is based on more simplistic morphological and kinematic assumptions; most of the above studies consider the more realistic, bar-dominated nature of the rotation curve. We also note that the ends of the arms are not clearly delineated in this galaxy.

4.0.3. NGC 157

Our estimate of $r_{\text{co}} \sim 56''$ agrees well with estimates in the literature based on detailed kinematic models. Sempere & Rozas (1997) find $r_{\text{co}} \sim 50''$, and Fridman et al. (2001) find $36'' < r_{\text{co}} < 63''$ by two different methods. Elmegreen et al. (1992) also estimate corotation to be at 56'' based on morphological arguments.

Spatial isochrones thus appear to offer a new technique for constraining the corotation radius for a first-order approximation. We can set a spatial correspondence between: (1) Corotation and the end of the nebular spiral arms; (2) Isochrone bunching and H II region clumps; and possibly (3) Outer Lindblad resonance and the edge of the star-forming disk. These physical coincidences suggest that the location of corotation has been identified to first order. Thus, while some authors often identified the ends of the star-forming arms with the corotation resonance, and others with the OLR, our analysis supports the former. We also note that in wide-format, blue photographic images available via the NASA/IPAC Extragalactic Database (e.g., from the Sandage-Bedke Atlas), there is no evidence in any of our galaxies that the dust lane crosses over from the inside to the outside of the arms at any point inside our adopted r_{co} .

5. CONCLUSION

To better understand the behavior of the H II LF and its ability to probe global star-formation properties, we have re-examined its relation to the H II region size distribution, and investigated its evolution with respect to density wave triggering in spiral galaxies.

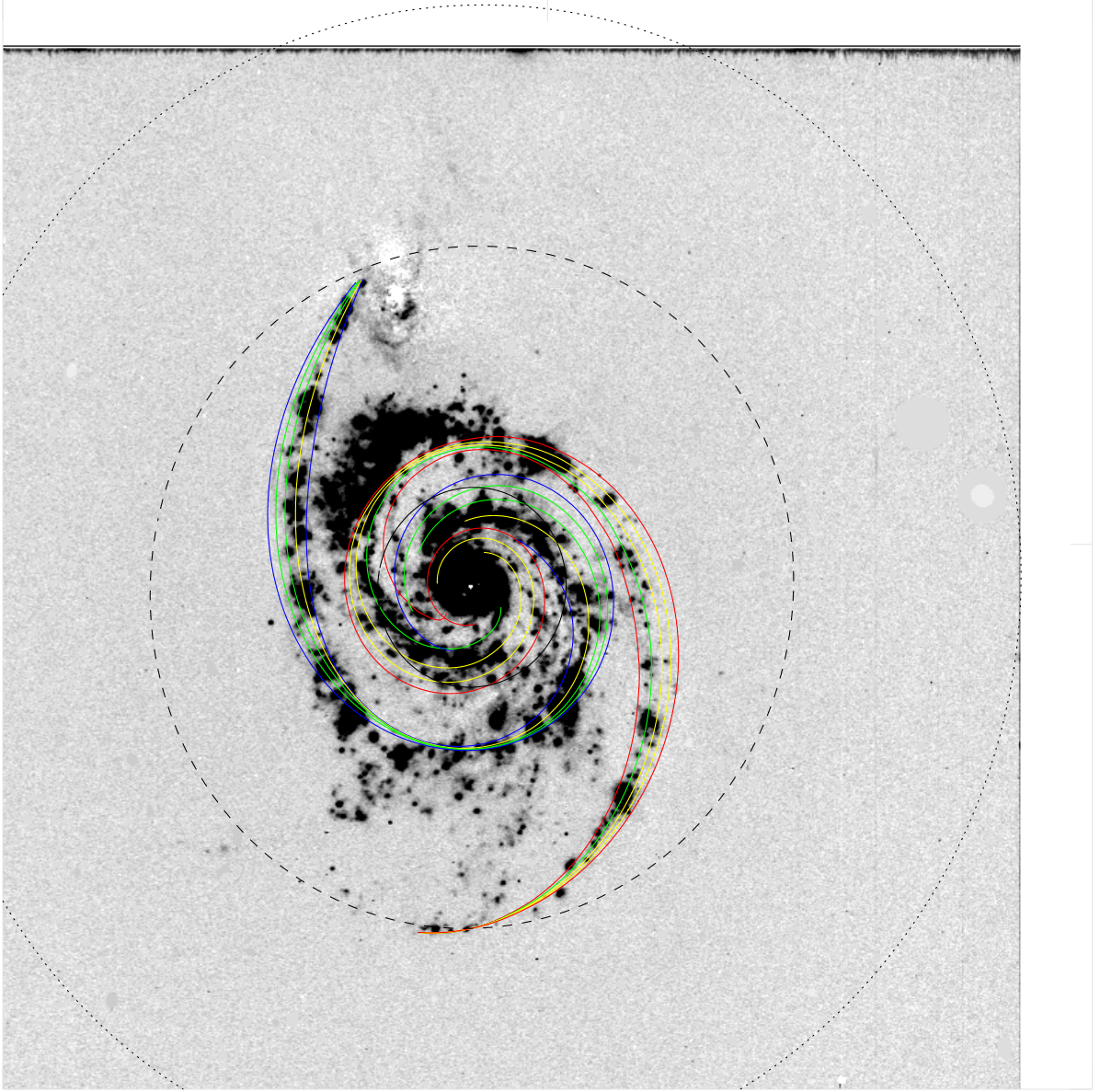


FIG. 7.— H α images of the sample galaxies, overlaid with spatial isochrones for -12 , 0 , 12 , 24 , and 36 Myr. These are respectively shown as red, green, yellow, yellow, red for one arm; and blue, yellow, green, green, blue for the other. The black dashed line shows the adopted corotation radius; the inner and outer Lindblad resonances are shown by the solid and dotted lines, respectively. Figure 7(a) shows M51, with H α data from Rand (1992).

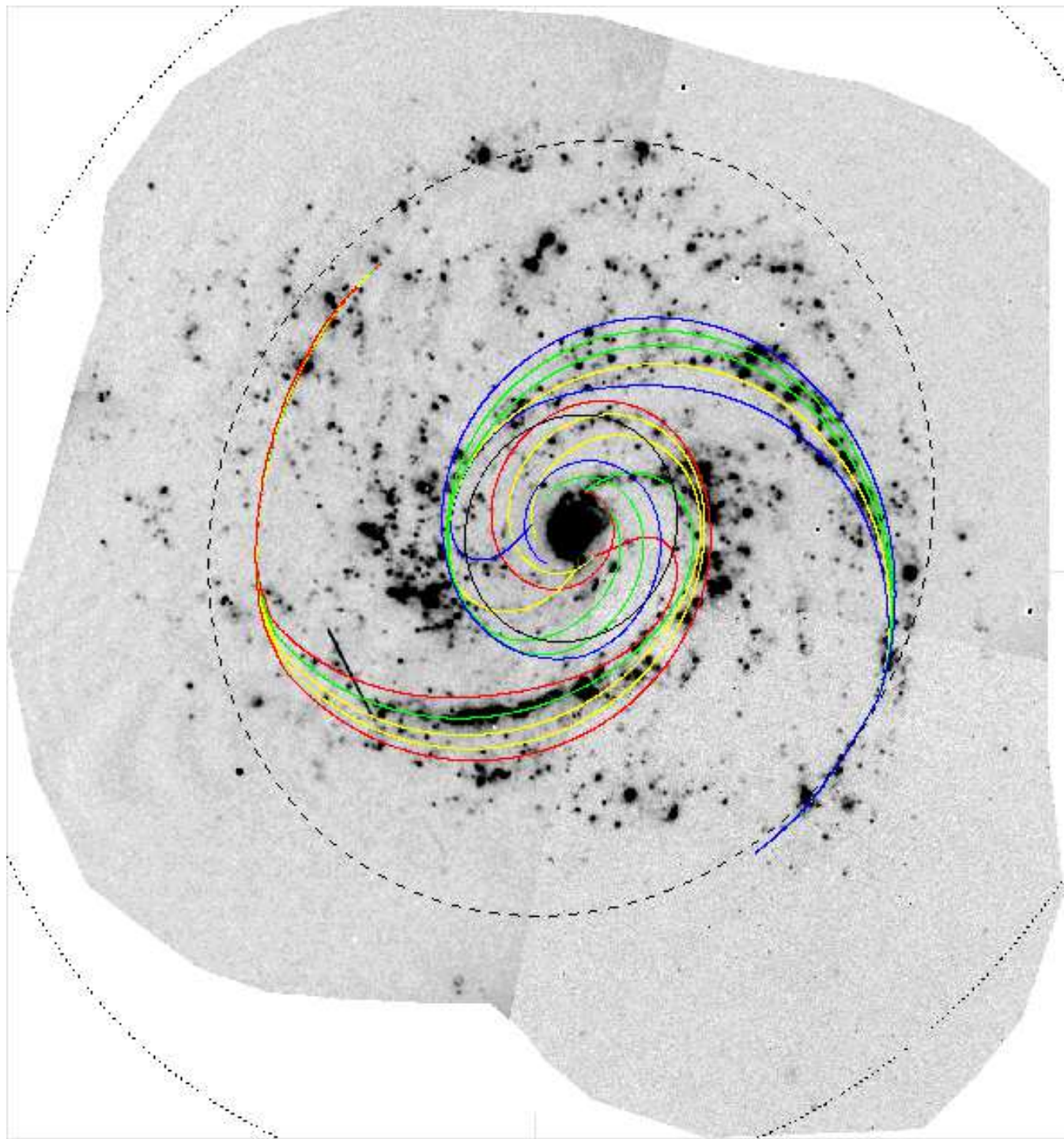


FIG. 7.— (b) M100; H α data from Knapen et al. 1993

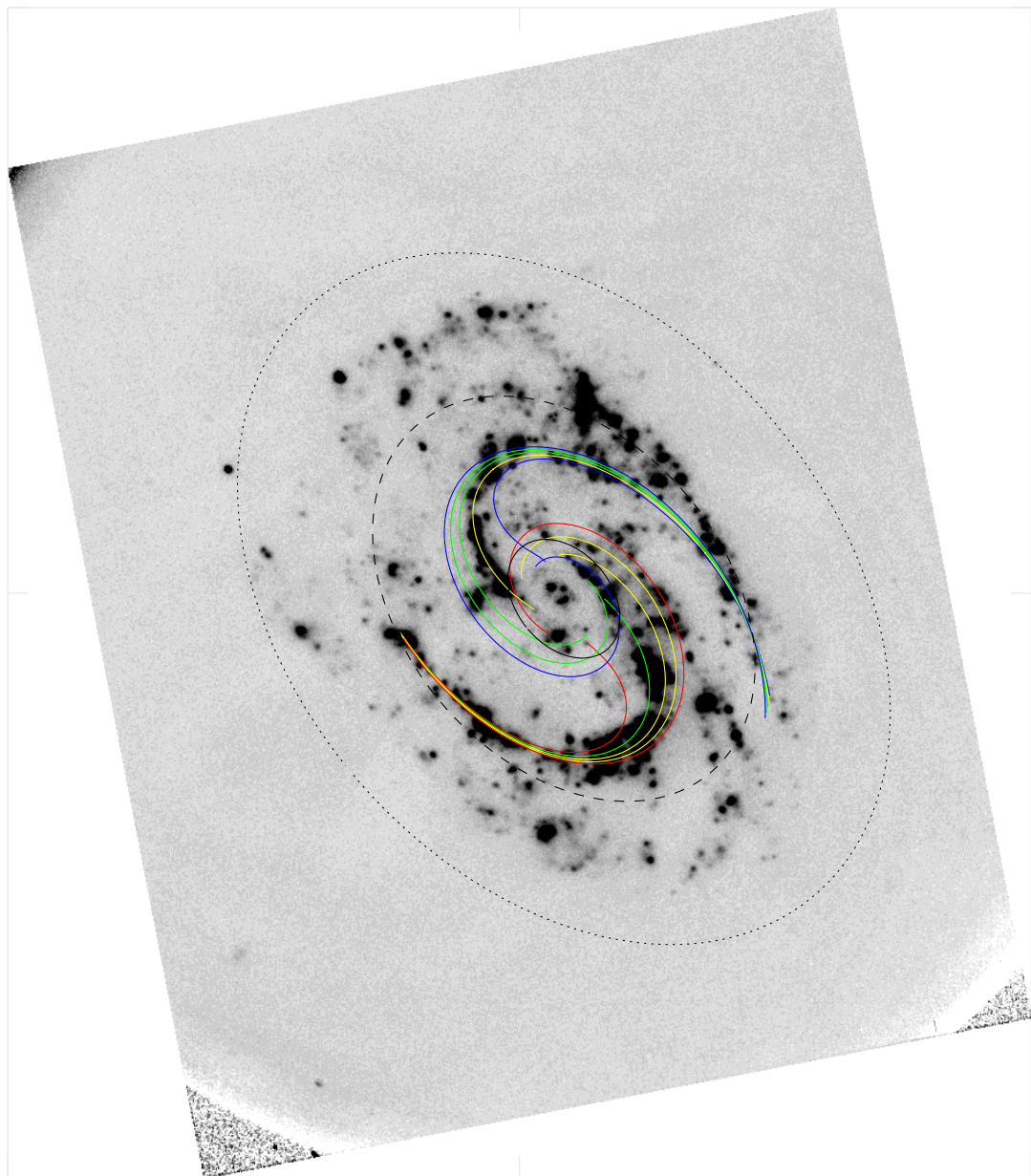


FIG. 7.— (c) NGC 157; H α data from Rozas et al. 1996

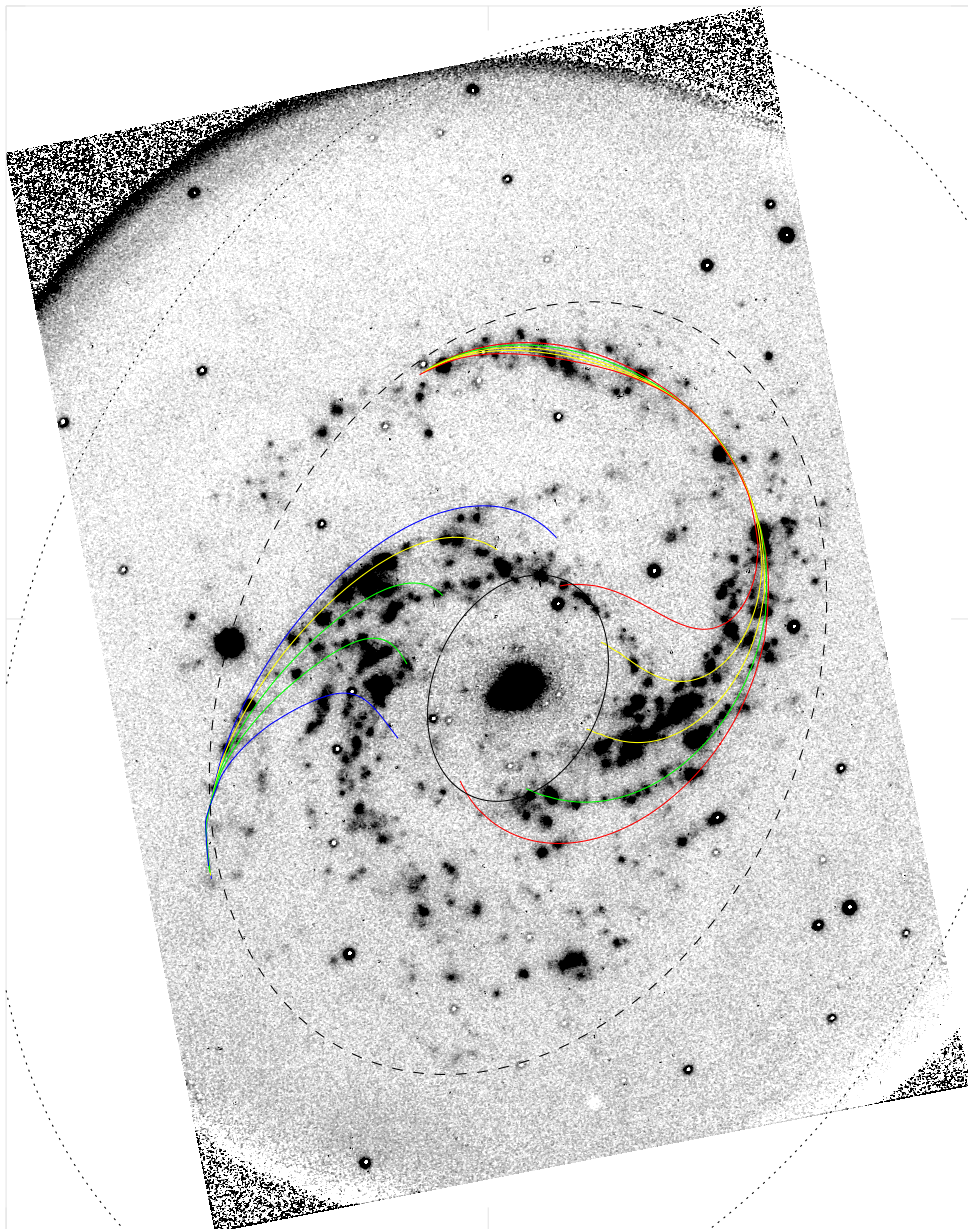


FIG. 7.— (d) NGC 6951; H α data from Rozas et al. 1996

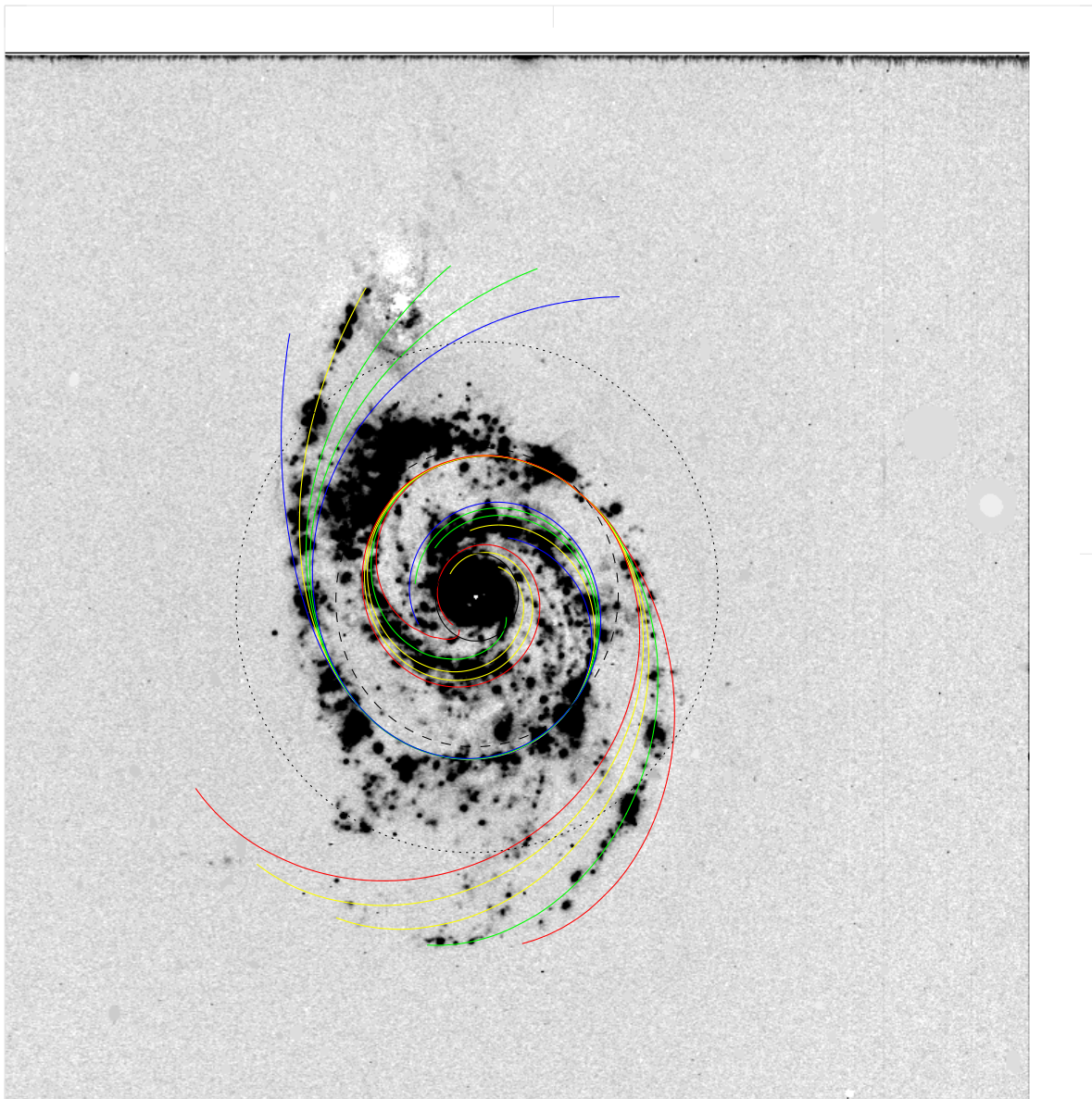


FIG. 8.— Same as Figure 7a, but with the M51 corotation at 9.6 kpc suggested by Elmegreen et al. 1992.

TABLE 2
GALAXY AND RESONANCE PARAMETERS

Galaxy	Distance (Mpc)	v_{circ} (km s^{-1})	r_{circ} (kpc)	r_{co} (kpc)	ILR (kpc)	OLR (kpc)	Reference ^a
M51	9.6	220	0.93	14	4.1	24.9	Rand (1993)
M100	16.1	210	1.56	12	3.5	20.5	Sempere et al. (1995)
NGC 157	22.2	170	0.54	6	1.8	10.2	Sempere & Rozas (1997); Ryder et al. (1998)
NGC 6951	19.0	235	0.46	10	2.9	17.1	Rozas et al. (2002)

^aReferences for rotation curve parameters: r_{circ} is the radius beyond which the circular velocity is taken to be constant, at value v_{circ} .

We have analytically re-evaluated the relationship between the H II LF and the H II region size distribution. We suggest that *the size distribution is intrinsically described as a power law*, as physically related to the H II LF, rather than its conventional description by an exponential relation. We find that the physical relation between nebular luminosity and size implies that the slopes of the size distribution b and the luminosity function a should be related as $b = 2 - 3a$. The normally observed value $a = 2$ thus yields $b = 4$, which we find to be consistent with observations. We find that the slope transition radius $\log R_{\text{sat}} \sim 2.1$ pc corresponding to the transition luminosity $\log L_{\text{sat}} \sim 38.5$ is also consistent with observations.

We have developed a code to compute spatial isochrones from the rotation curve, given the current locus of the spiral density waves. Our code allows quantitative comparison of the nebular spatial distribution with the spatial isochrones. We find that the best correspondence for the arm H II regions occurs when the corotation radius coincides with the ends of the star-forming arms. This value for r_{co} also yields a coincidence between the Inner Lindblad Resonance with the radial onset of star formation in the arms for three of the four galaxies. There may also be a hint that the Outer Lindblad Resonance coincides with the outer edge of the star-forming disk in at least one galaxy. *The spatial isochrones therefore appear to offer a new technique for determining the corotation radius and principal resonances.*

We had hoped that these isochrones would isolate subsets of H II regions that could then be used to study evolutionary effects of the nebular population. However, for three of the four galaxies, the isochrones do not yield adequate spatial separation over the nebular evolution timescale, relative to the spatial scatter at any given age. Encouragingly, we do find that the spatial concentration of the objects along the isochrones is consistent with the overall nebular evolutionary timescale in these galaxies. However, the data do suggest periods of extended star formation at any given location that blur the diagnostics. Combined with uncertainties in the kinematic parameters, this greatly limits the ability to obtain clear quantitative constraints on H II LF evolutionary parameters as related to the density wave passage. The observed rate of evolution, however, does set limits on the importance of this process in producing the observed arm-interarm variation in the H II LF.

We are pleased to acknowledge useful discussions with Ron Allen and Blaise Canzian, and also comments from the anonymous referee. Johan Knapen, Rich Rand, and Maite Rozas kindly provided their H α observations of the galaxies studied here. We thank Laura Woodney for tips with IDL. Much of this work was carried out by the PI while at the Space Telescope Science Institute, and by JSP and VJM under the STScI Summer Student Program. MSO also acknowledges support from the National Science Foundation, grant AST-0204853. XZ is supported in part by funding from the Office of Naval Research.

REFERENCES

Banfi M., Rampazzo R., Chincarini G., & Henry R. B. C., 1993, *A&A*, 280, 373

Canzian, B. 1993, *ApJ*, 414, 487

Canzian, B. & Allen, R. J. 1997, *ApJ*, 479, 723

Cepa, J. & Beckman, J. E. 1990, *ApJ*, 349, 497

Cioffi D. F. & Shull J. M. 1991, *ApJ*, 367, 96

Clemens, M. S., & Alexander, P. 2001, *MNRAS*, 321, 103

Elmegreen, B. G., Elmegreen, D. M., & Montenegro, L., 1992, *ApJS*, 79, 37

Elmegreen, B. G., Elmegreen, D. M., & Seiden, P. E. 1989, *ApJ*, 343, 602

Elmegreen, B. G., Wilcots, E. & Pisano, D.J. 1998, *ApJL*, 494, 37

Fridman, A. M., et al. , 2001, *A&A* 371, 538

García-Burillo, S., Combes, F., & Gerin, M. 1993b, *A&A* 274, 148

García-Burillo, S., Guélin, M., & Cernicharo, J. 1993a, *A&A* 274, 123

García-Burillo, S., Sempere, M. J., Combes, F., & Neri, R. 1998, *A&A* 333, 864

Kenney, J. D. P., Wilson, C. D., Scoville, N. Z., Devereux, N. A., & Young, J. S. 1992, *ApJ* 395, L79

Kennicutt R. C., Edgar B. K., & Hodge P. W., 1989, *ApJ*, 337, 761

Knapen J. H., 1998, *MNRAS*, 297, 255

Knapen J. H., Arnth-Jensen N., Cepa J., & Beckman J. E., 1993, *AJ*, 106, 56

Knapen J. H., Beckman J. E., Cepa J., van der Hulst, T., & Rand, R. J. 1992, *ApJ*, 385, L37

Lin, C.C. 1970, in *The Spiral Structure of Our Galaxy*, W. Becker & G. I. Contopoulos (eds.), IAU Symp. 38, (Dordrecht: Reidel), 377

Oey M. S. & Clarke C. J. 1998, *AJ*, 115, 1543; (Paper I)

Panagia N. 1973, *AJ*, 78, 929

Pleuss, P. O., Heller, C. H., & Fricke, K. J., 2000, *A&A*, in press, astro-ph/0010565

Rand R. J., 1992, *AJ*, 103, 815

Rand R. J. & Kulkarni 1990, *ApJ*, 349, L43

Rohlf, K. 1977, *Lectures on Density Wave Theory* (Heidelberg: Springer), 95

Rozas M., Beckman J. E., & Knapen J. H. 1996, *A&A*, 307, 735

Rozas M., Knapen J. H., & Beckman J. E. 1996b, *A&A*, 312, 275

Salpeter E. E. 1955, *ApJ*, 121, 161

Sandage, A. & Bedke, J. 1988, *NASA SP-496*, (Washington: NASA)

Sandage, A. & Tamman, G. A. 1987, *A Revised Shapley-Ames Catalog of Bright Galaxies*, 2nd Edition, (Washington: Carnegie Institution of Washington)

Schaerer D., de Koter A. 1997, *A&A*, 322, 598

Sempere, M. J., García-Burillo, S., Combes, F., & Knapen, J. H., 1995, *A&A*, 296, 45

Sempere, M. J. & Rozas, M. 1997, *A&A*, 317, 405

Shu, F. H., Stachnik, R. V., & Yost, J. C. 1971, *ApJ*, 166, 465

Vacca W. D., Garmany C. D., & Shull J. M. 1996, *ApJ*, 460, 914

Thilker, D. A., Walterbos, R. A. M., Braun, R. & Hoopes, C. G. 2002, *AJ*, 124, 3118

Tremaine, S., & Weinberg, M.D. 1984, *ApJL*, 282, 5

van den Bergh, S., 1981, *AJ*, 86, 1464

Vogel, S. N., Rand, R. J., Gruendl, R. A., & Teuben, P. J. 1993, *PASP*, 105, 666

Youngblood, A. J. & Hunter, D. A. 1999, *ApJ*, 519, 55

Zhang, X., Wright, M., & Alexander, P. 1993, *ApJ*, 418, 100